

Methodology for Scale-Resolving Simulation of Unsteady Effects in Turbomachines

Alexey P. Duben¹ , Viacheslav A. Sapozhnikov¹ 

© The Authors 2025. This paper is published with open access at SuperFri.org

Methodology for studying effects associated with periodic unsteady impact of neighbouring rows in turbomachines is presented. The two-stage procedure of an investigation is as follows: simulation using an approach based on solving the Reynolds-averaged Navier–Stokes equations (RANS) of an entire turbomachine at the first stage and scale-resolving simulation (SRS) of a particular row at the second. The methodology exploits the following methods and technologies, which are implemented in the NOISEtte computational algorithm: the nonlinear harmonics method as a RANS approach to obtain unsteady inflow parameters for SRS; the hybrid Improved Delayed Detached Eddy Simulation approach for SRS of the row under detailed study. SRS considers using the dynamic synthetic turbulence generator in a form of volumetric source terms (VSTG) to reproduce unsteady periodic turbulent perturbations. A dynamic version of the VSTG, the parameters of which depend on the flow upstream the source region, is formulated. Details of the parallel heterogeneous implementation of the dynamic VSTG are discussed. To demonstrate the applicability of the presented methodology, a simulation of non-stationary effects in a cascade of T106 low-pressure turbine blades was performed.

Keywords: turbulent flows, non-linear harmonics method, scale-resolving simulation, hybrid RANS-LES approach, IDDES, CPU+GPU, MPI+OpenMP+OpenCL, synthetic turbulence.

Introduction

Increasing performance of computing resources and development of high-fidelity numerical models, methods, and algorithms for CFD (Computational Fluid Dynamics) promotes further engagement of scale resolving simulations (SRS) for solving turbomachinery problems [21, 29]. In terms of modeling approaches, either direct numerical simulation (DNS) or wall-resolved large-eddy simulation (WRLES) are mainly used due to the complex physical phenomena and flow specifics that significantly affect the turbine or compressor performance (e.g., integral ones such as total pressure losses or efficiency). The most impactful are the following: inflow turbulence parameters, laminar-turbulence transition on the suction side of a blade, the influence of upstream unsteady perturbations caused by wakes from the previous row. Simulations are usually carried out for simplified configurations like a plane-parallel blades cascade. Unsteady RANS (URANS) and hybrid RANS-LES methods are exploited for high Reynolds number flows over more industrial configurations, e.g., simulations of the bypass duct of a turbofan engine [23, 28]. Most investigations of a plane-parallel blades cascade (e.g., see [8, 15, 22]) consider homogeneous inflow conditions by maintaining a specified turbulence intensity level. One of the necessary components accompanying scale-resolving simulation for such investigations is a technique for creating unsteady turbulent pulsations. It allows to replicate adequate flow characteristics upstream a blade under consideration. The impact of unsteady flow features, namely, wakes coming from the previous stage, is less frequently studied. For instance, the T106 low-pressure turbine (LPT) blades cascade was investigated using SRS in [11, 18, 32]. The test case is based on the corresponding experimental data [27]. The incoming wakes produced by the moving bars in the experiment, were simulated either artificially in [18, 32] or directly [11]. In the latter, the flow behind the moving bars was modeled with a sliding interface to transfer the induced perturbations to the domain with the T106 blade. This methodology is practically not applicable to

¹Keldysh Institute of Applied Mathematics, RAS, Moscow, Russian Federation

industrial configurations, because consideration of an upstream row in SRS increases the cost of the computation by several times, which is prohibitive given the already significant cost for a row. Thus, a feasible technique should engage a technology for creating artificial pulsations.

The most efficient and widespread solution to consider turbulent characteristics of the incoming flow is to inject artificially generated pulsations of velocity. Among this class of techniques the synthetic turbulence generator (STG), presented in [25], is considered to be quite an impactful comprehensive solution ready for practical applications. Its most advantageous feature is a possibility to obtain adequate turbulent fields at a relatively small distance downstream the source region (also called “relaxation distance”). For instance, the relaxation distance for boundary layer turbulence usually varies between 3 and 5 of its thicknesses, which is relatively small. This feature is essential for turbomachinery because blade rows are mounted close to each other. STG was formulated initially for the form of inlet boundary conditions and adjusted to replicate boundary layer and shear layer turbulence. In [24], a methodology of its injection as a distributed volume source (Volume STG, VSTG) was proposed. The flow in the highly loaded T106C turbine cascade with different turbulent inflow conditions was investigated [8] by authors of the present paper earlier. The VSTG was used there to reproduce an intake with a turbulence level of 3%.

We present a methodology for studying effects associated with periodic impact of wakes from the preceding row in turbomachines using SRS based on the dynamic VSTG. An essential part of it is the nonlinear harmonics (NLH) method, implemented [7, 10] in NOISEtte [2, 13], which is used to obtain unsteady inflow parameters in a preliminary RANS computation. In contrast to the mixing plane technology [5, 9], which assumes circumferential uniformity, NLH allows modeling of unsteady effects that are related to the blade-passing frequency of adjacent rows. Thus, the time-dependent RANS solution can be restored and set in the form of an unsteady boundary condition at the rotor-stator interface upstream the row which is being investigated using SRS. In turn, VSTG is adapted to the capabilities of dynamically varying turbulent flow downstream of the source region. We use the T106 LPT cascade, which is investigated in [11, 18, 32], to demonstrate performance of the technology.

The paper is organized as follows. Section 1 presents short overview of mathematical models and numerical methods implemented in the NOISEtte algorithm that are used for simulations. Section 2 presents an overview of the proposed methodology. Section 3 is dedicated to the dynamic version of VSTG including its parallel implementation and testing on a turbulent mixing layer flow, which is similar to a wake downstream a turbomachine blade. Section 4 presents the simulation results of the flow over T106A low-pressure turbine blades to demonstrate the performance of the technology. Conclusion summarizes the results of the work.

1. NOISEtte: Mathematical Models and Numerical Methods

The numerical algorithm realized in the NOISEtte [2, 13] research code is based on the Navier–Stokes equations for a compressible perfect gas.

We use the latest version of the hybrid non-zonal RANS-LES method IDDES [14] as an SRS approach. Despite the fact that the flow over the T106 blade is actually simulated in LES regime (we use a mesh with proper resolution), the RANS branch is required in the region downstream the inlet boundary and upstream the VSTG source to conduct unsteady RANS solution (see Section 2 for details). We use the recent version of the IDDES based on the Menter $k - \omega$ SST model [17] and Δ_{SLA} [19, 26] dynamic subgrid scale.

NOISEtte is a vertex-centered code on mixed-element unstructured meshes. It is based on the edge-based reconstruction scheme EBR [3], which provides higher accuracy for approximation of convective fluxes. The method of averaged element splittings (AES) [4] is used for discretization of the diffusion terms.

The 2nd order numerical scheme based on the backward differentiation formula is used. The BDF1 was applied for RANS simulations and BDF2 for SRS. To solve nonlinear algebraic systems, a simplified Newton method is used, and the linear systems are solved using the BiCGStab solver [20] with Gauss–Seidel method-based parallel preconditioner [16].

The parallel implementation of NOISEtte is based on MPI, OpenMP and OpenCL frameworks. The heterogeneous parallel algorithm and its implementation are described in detail in [13]. All simulations were carried out on GPUs.

2. Overview of the Methodology

The methodology is as follows (see Fig. 1 for visualization). Let us consider that a multi-stage turbomachine is being examined, and a particular row, either rotor or stator, is needed to be thoroughly investigated using SRS (a rotating row in Fig. 1). Thus, the study is divided into two sequential stages.

1. RANS+NLH simulation of an entire turbomachine (RANS+NLH stage).
2. SRS simulation of a separate row with unsteady boundary conditions and the dynamic VSTG (SRS stage).

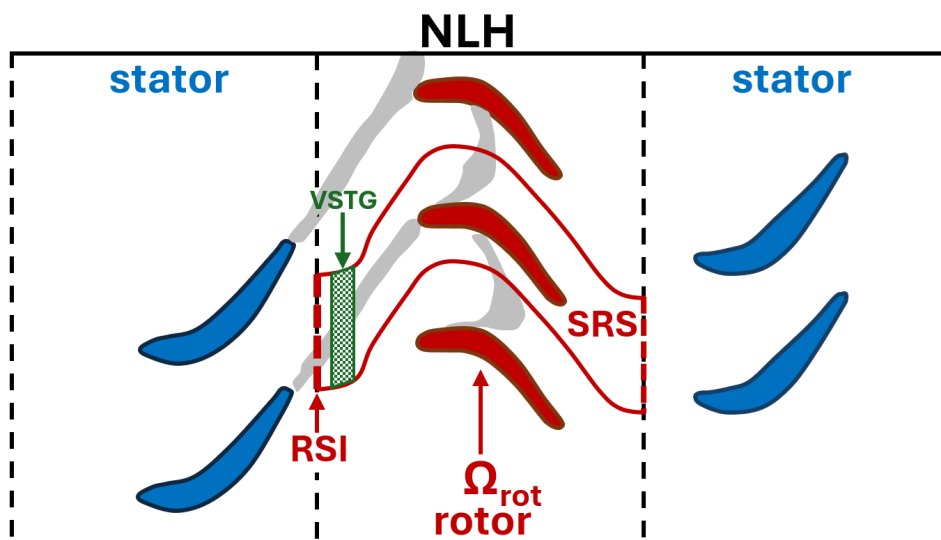


Figure 1. Sketch of the two-stage methodology

The main goal of the first stage is to obtain unsteady inflow characteristics, which reproduce flow dynamics of the adjacent upstream row, mainly, wakes past the corresponding blade. The simulation using NLH assumes only one vane channel per row with periodic boundary conditions in the circumferential direction. As result of the computation, those distributions can be extracted at every rotor-stator interface (RSI): averaged flow distributions of fields; Fourier coefficients from an adjacent row, the perturbations of which are approximated using the flow decomposition. Passing through the RSI, the stationary fields with respect to one stage turn into unsteady fields relative to the adjacent domain, which rotates at a different speed. The corre-

sponding formulas are given in [7]. Here we provide the formulas for the simplified configuration that we consider (see Section 4).

The second stage assumes scale-resolving simulation of the row under consideration (see SRS region in Fig. 1). The VSTG is imposed downstream the inlet boundary and upstream the blade. All the required data for it could be obtained from the solution using RANS+NLH. The target solution for the sponge layer can be extracted too. It is needed to properly dump perturbations downstream the blade till the outlet boundary. Besides the NLH for the first stage, another important part of the methodology is the involvement of Detached Eddy Simulation (DES) for the SRS stage. The reason is that, operating within the RANS regime, it allows to conduct unsteady periodic pulsations from the inlet boundary downstream towards the VSTG region. More specifically, the IDDES approach [14] is the most eligible because it switches to SRS near walls in the presence of resolved turbulence, either WRLES or WMLES (Wall-Modelled LES), depending on the mesh resolution.

Both RANS+NLH and SRS stages assume consideration of one vane channel per row. But, in case of non-multiplicity of the number of blades in adjacent rows, which is a common practice for turbomachines, performing the SRS stage seems complicated. As for the RANS+NLH stage, harmonic amplitudes for a domain are treated using the generalized periodicity BC with phase shift. There are two options to deal with the non-multiplicity problem. The first is to slightly change, namely, rescale, the geometry of a turbomachine, so that the number of blades in the rows became a multiple, that, for instance, was done in [31]. This should not significantly affect the aerodynamics, but allows the proposed technique to be used for a detailed study of unsteady effects, with only one vane channel being resolved by the corresponding computational mesh. The second option is to implement a generalized periodicity BC with phase shift for SRS.

3. Unsteady VSTG

3.1. Formulation

The VSTG [24] involves adding pulsations as source terms for a node, defined by the radius-vector $\mathbf{r} = (x, y, z)$, to the momentum and energy equations by the following form

$$\mathbf{F}(\mathbf{r}) = C_{\text{VSTG}}\rho U_0 \mathbf{u}'(\mathbf{r})\alpha(\mathbf{r}), \quad (1)$$

where $C_{\text{VSTG}} = 1.1$ is empirical constant, $\rho = \rho(\mathbf{r})$ is density, U_0 is characteristic convective velocity inside the source region, $\mathbf{u}' = \mathbf{u}'(\mathbf{r})$ is the vector of velocity fluctuations computed using the STG [25], $\alpha(\mathbf{r})$ is a weight function constructed so that its integral value along the streamwise direction (denote it by τ_{sw}) throughout the source region equals to 1. An example of the source region is depicted as ‘‘VSTG’’ in Fig. 1. Also, the transport equation for the turbulence kinetic energy k is extended by the source term too:

$$F_k(\mathbf{r}) = -\rho U_0 \alpha(\mathbf{r}) \omega \max(\nu_t^{\text{SRS}} - \nu_t^{\text{SMG}}, 0), \quad (2)$$

where $\omega = \omega(\mathbf{r})$ is the specific turbulence dissipation rate, $\nu_t^{\text{SRS}} = \nu_t^{\text{SRS}}(\mathbf{r})$ is actual turbulence viscosity, $\nu_t^{\text{SMG}} = \nu_t^{\text{SMG}}(\mathbf{r})$ is Smagorinsky eddy viscosity.

According to the STG formulation [24, 25], time-dependent velocity pulsations are calculated as

$$\mathbf{u}'(\mathbf{r}, t) = A_{ij} \mathbf{v}'(\mathbf{r}, t), \quad \mathbf{v}'(\mathbf{r}, t) = 2\sqrt{(3/2)} \sum_{n=1}^{N_m} \sqrt{q^n} [\boldsymbol{\sigma}^n \cos(k^n \mathbf{d}^n \cdot \mathbf{r}' + \phi^n)], \quad (3)$$

We define the pseudo-position vector \mathbf{r}' in (3) for the node with radius-vector \mathbf{r} as

$$\mathbf{r}' = \{\xi', \eta', \zeta'\}, \xi' = \frac{2\pi(\mathbf{r} \cdot \boldsymbol{\tau}_{\text{sw}} - U_0 t)}{k^n \max\{l_e(\mathbf{r})\}}, \eta' = \mathbf{r} \cdot \boldsymbol{\tau}_{\text{tr}}, \zeta' = \mathbf{r} \cdot \boldsymbol{\tau}_{\text{sp}}. \quad (4)$$

$\max\{l_e(\mathbf{r})\}$ in (4) is a function of l_t and the distance to the wall. The formulation (4) is similar to the original formulation of \mathbf{r}' as shown in formula (5) of [25]. It is transformed into this form when the $\boldsymbol{\tau}_{\text{sw}}$ direction is aligned with the positive direction of the OX axis.

The following parameters are updated during the simulation (they are taken from reference nodes $\{i_f^{\text{ref}}\}$) when a non-stationary periodic flow upstream the source region is considered: R_{ij} and l_t .

Note that Shorstov [23] slightly modified the formulation (4) to provide adequate velocity scales inside the source region: spatially variable distribution of convective velocity was assumed instead of a single velocity scale U_0 . This option was implemented, but was not used for the simulations presented in this paper, because it did not affect the turbulence generated by the VSTG.

3.2. Parallel Implementation

The dynamic VSTG was implemented in both CPU and GPU versions of the finite-volume computational algorithm for unstructured meshes, implemented in the parallel heterogeneous code NOISEtte [2, 13]. The kernels realizing all computationally intensive procedures are incorporated in the GPU version.

All data required for VSTG operation is initialized before time stepping. Note that reference nodes, which contain values needed to calculate R_{ij} and l_t , could not belong to the same MPI domain as a VSTG node, in which artificial pulsations are generated. Thus, updating of these defining parameters requires global MPI synchronization of all parallel processes. However, it takes a negligible amount of time because the number of the reference nodes is very small.

The number of VSTG nodes is orders of magnitude smaller (usually it is about several percent) than the number of mesh nodes. But they are distributed among MPI processes in a highly unequal way, which of course leads to load imbalance. Moreover, the computational load for a single VSTG node is quite large due to the cycle on harmonics (see equation (3)), which can number in hundreds. As practice has shown, calculations implementing the formulas (1)–(3) take on average about several percent of the time spent on processing the entire step.

The implementation of the dynamic version of VSTG revealed a similar problem to the one mentioned in [12]. Initially, updating VSTG node parameters, namely, R_{ij} and l_t , was implemented entirely on the CPU. It led to the situation that this procedure occupied a significant part of the step (tens of percent). The most computationally intensive procedure that slows down the computation is the recalculation of normalized mode amplitudes $\{q^n\}_{n=1}^{N_m}$ for each VSTG node: its load is comparable to the calculation of source terms according to the formulas (1)–(3). The static VSTG requires this cycle to be run only once per computation during initialization, which is done entirely on the CPU. Therefore the recalculation of normalized mode amplitudes was ported to the GPU too. As a result, only operations related to MPI exchanges remained on the CPU, and the costs of dynamic VSTG operations do not exceed a few percent of the total time step. This value can be reduced if the VSTG node parameters are not updated at every time iteration.

3.3. Testing on a Mixing Layer

The LaRC Turbulence Modeling Resource (TMR) 2D Mixing Layer case [1] is used for validation of the VSTG in the static mode. Schematics of the flow configuration and simulation set-up is presented in Fig. 3. It is characterized by the following parameters: ambient pressure $P_\infty = 101325$ Pa, temperature $T_\infty = 293$ K, the freestream velocities are $U_1 = 41.54$ m/s and $U_2 = 22.4$ m/s, the Reynolds number based on U_1 and $L = 1$ m is $Re = 2.76 \cdot 10^6$. The results are evaluated using the experimental data [6].

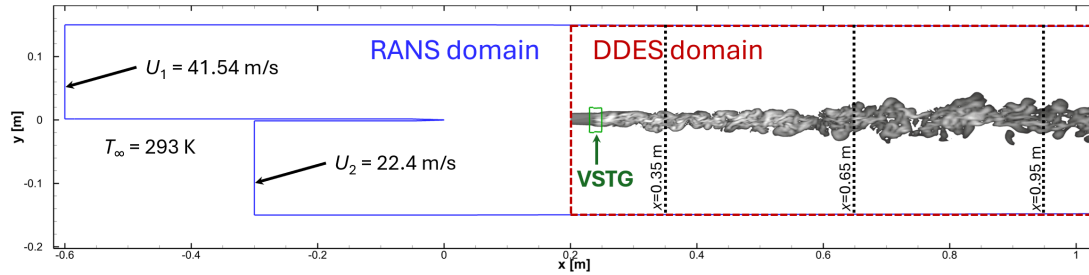


Figure 3. Mixing layer: schematics of the flow configuration and simulation set-up

The simulations were carried out in two stages. 2D SST RANS solution was obtained at the first stage using a low-Reynolds mesh (wall-normal mesh step $\Delta_{y,1}^+ < 1$) taken from [1]. The computational domain (see RANS domain in Fig. 3) fits into a rectangle $-0.6 \leq x/L \leq 1.2$ and $-0.15 \leq y/L \leq 0.15$, the trailing edge is located at $(0, 0)$. The freestream velocities were set at the inlet: the upper one is at $x/L = -0.6$, the lower one – at $x/L = -0.3$. Ambient pressure was prescribed at the outlet. The walls of the plate were treated as adiabatic no-slip. At the second stage, the DDES [14] simulation was carried out using the 3D mesh containing 7.61 M nodes (220 nodes in the spanwise direction, along OZ axis). The profiles obtained using 2D SST RANS were imposed at the inlet, which is located at $x/L = 0.2$ (see DDES domain in Fig. 3). The outlet boundary was extended till $x/L = 2$. The streamwise mesh step starts from $\Delta_x/L = 10^{-3}$ till $\Delta_x/L = 4 \cdot 10^{-3}$ at $x/L = 1.1$, and coarsens towards the outlet boundary. The transverse mesh step starts from $\Delta_y/L = 1.5 \cdot 10^{-4}$ till $\Delta_y/L = 6 \cdot 10^{-4}$ at $x/L = 1.1$ along the line $y = 0$, and coarsens towards the outlet boundaries. The spanwise mesh step is $\Delta_z/L = 5 \cdot 10^{-4}$. The VSTG was imposed inside the region $0.23 \leq x/L \leq 0.25$, the reference nodes are located $l_{us}/L = 0.01$ upstream.

An instantaneous snapshot of the vorticity magnitude from the SRS simulation is shown in Fig. 3 (see visualisation within the DDES domain). The flow in the mixing layer becomes plausibly turbulent rather quickly: the length of the relaxation period does not exceed its several thicknesses. Averaged streamwise velocity profiles and Reynolds stresses are presented in Fig. 4. Note that the $x/L = 0.35$ profile corresponds to a location approximately $6\delta_{\omega 0}$ downstream the VSTG zone ($\delta_{\omega 0}$ is the vorticity thickness at $x/L = 0.2$). It can be seen that the SRS distributions are close to both the experimental data and the RANS solution. The shape of the graphs is captured properly, while peak values are slightly overestimated at $x/L = 0.65$.

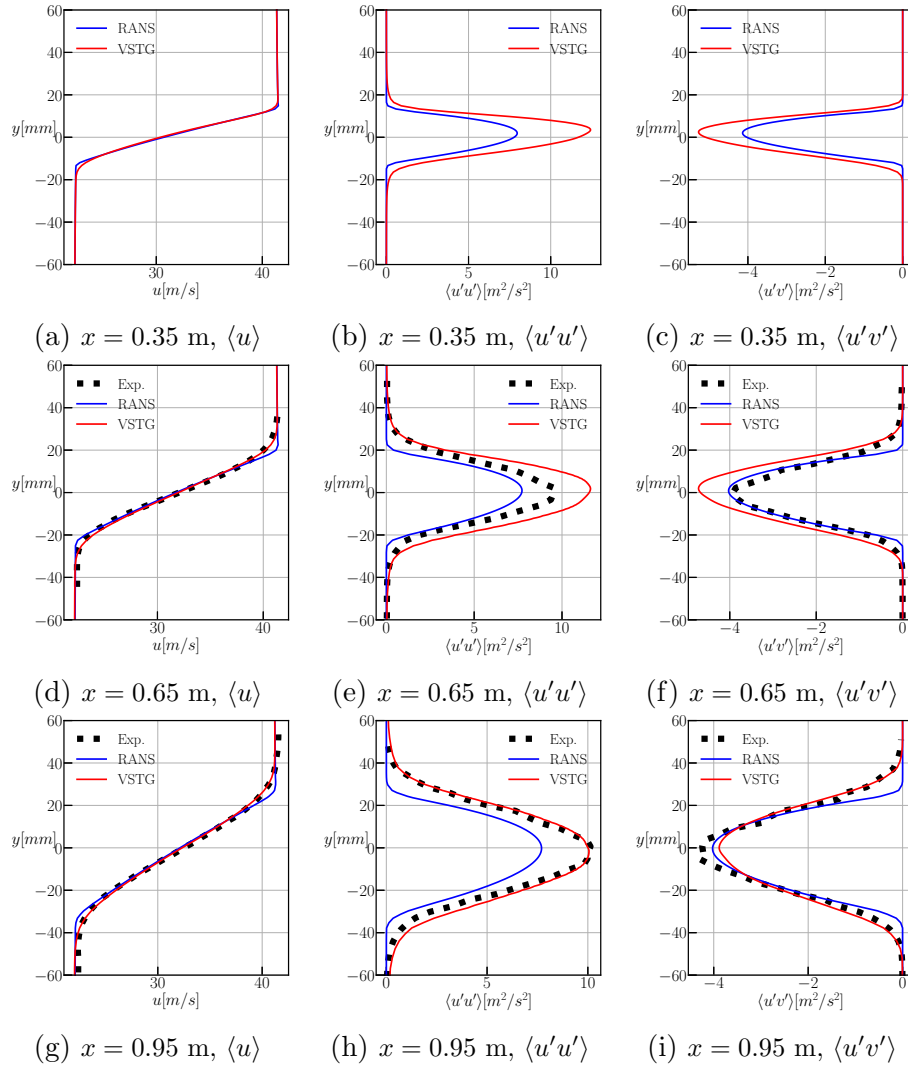


Figure 4. Mixing layer: profiles of averaged streamwise velocity and Reynolds stresses

4. Unsteady Flow over the T106 LPT Cascade

4.1. Computational Setup

The test case corresponds to an experimental LPT linear rig [27] with the following geometrical details: inlet flow angle 45.5° , axial chord $C_x = 0.86C$ (C is chord), pitch $P = 0.799C$. The T106 LPT cascade was investigated in [11, 18, 32], there is reference data for both steady (without turbulent income) and unsteady regimes. The following parameters define the flow over the T106 cascade: isentropic exit Mach number $\text{Ma}_{2\text{nd}} = 0.4$, Reynolds number based on C and exit velocity u_{out} (hereinafter also denoted as u_{ref}) is $9.8 \cdot 10^4$. The Reynolds number based on the inlet velocity u_{in} is $5.1 \cdot 10^4$. The blade aspect ratio is 1.76, thus the flow is considered to be nearly two-dimensional at mid-span. Schematics of the flow configuration and simulation set-up is visualized in Fig. 5. The inlet boundary is located at $x/C = -0.35$, the outlet – at $x/C = 2.05$. The point $(x, y) = (0, 0)$ corresponds to the leading edge of the blade.

The effect of an upstream blade row is simulated by a moving cylinder wake generator (moving bars) with a cylinder diameter $d = 0.02C$. The bars located at C_x upstream the leading edge of the T106 blade move with tangential velocity $u_{\text{bar}} = 0.41u_{\text{in}}$ along the OY axis down-

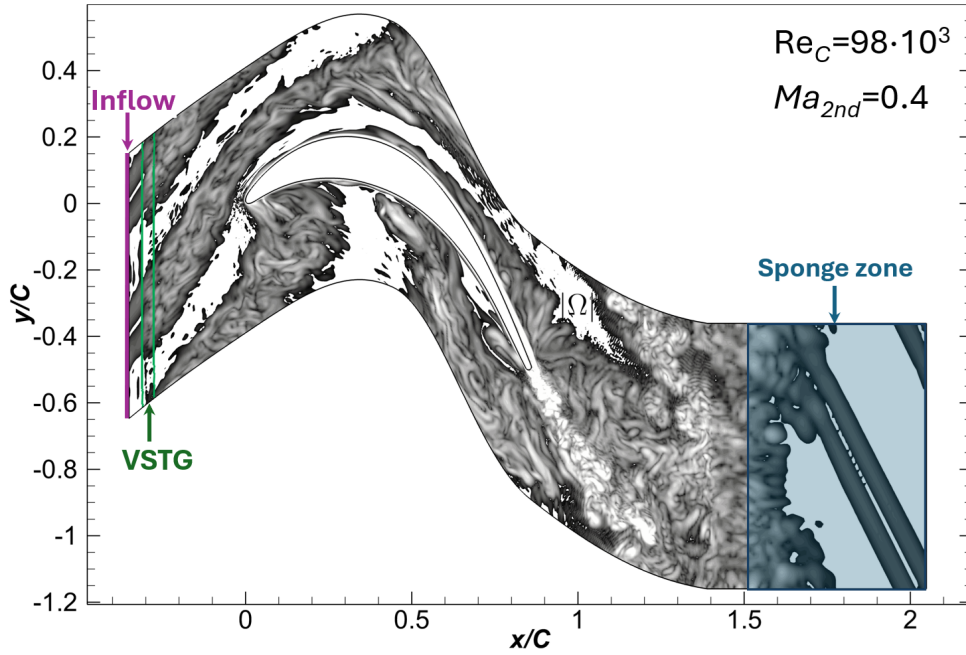


Figure 5. T106: schematics of the flow configuration and simulation set-up

ward y . It is considered that blades do not affect the flow over bars, so we simulate the flow over bars separately. The computational domain for the bars (see Fig. 6 top) is aligned with the coordinate system for the blade. It is two times smaller along OY due to the fact that there are two cylinders per pitch P and ranges from $-1.72C$ to $1.032C$ along the OX axis. RANS computation was performed in the coordinate system associated with the moving cylinders.

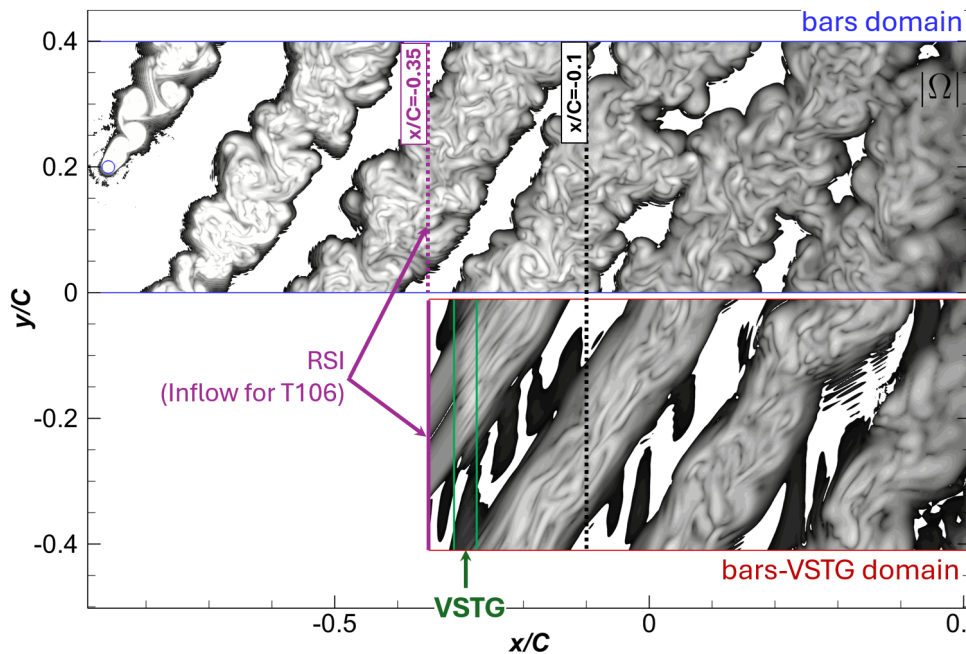


Figure 6. Moving bars: schematics of the flow configuration and simulation set-up (a fragment of the bars domain at the top and of the bars-VSTG domain at the bottom)

The following boundary conditions were applied in simulations: specified total pressure P_t , total temperature T_t , flow direction and turbulence characteristics (k and ω) at the inflow

boundaries; static pressure p at the outlet; periodicity along y and z directions. To generate data for providing the unsteady boundary conditions for the SRS computation, the RANS solution of the bars configuration at cross section $x/C = -0.35$ was decomposed by N_h spatial harmonics with base wave number $2\pi/P$ (first harmonic). It was done for P_t , T_t , k and ω , but not for flow directions due to their negligible variation. The fundamental frequency of relative periodic flicker (actually, the blade passing frequency) of these spatial perturbations from bars is equal to $\Omega_{\text{bar}} = 2\pi P/u_{\text{bar}}$. Having Fourier coefficients $\{\tilde{Q}_j^a + i\tilde{Q}_j^b\}_{j=0}^{N_h}$ (i is the imaginary unit) for the variable Q , its instantaneous value $Q(y, t)$ (it depends on the spatial coordinate y and time t) at the inlet boundary is calculated by the formula

$$Q(t, y) = \bar{Q} + \sum_{j=1}^{N_h} \left[\left(\tilde{Q}_j^a \cos(sj) + \tilde{Q}_j^b \sin(sj) \right) \cos(\tau j) + \left(\tilde{Q}_j^b \cos(sj) - \tilde{Q}_j^a \sin(sj) \right) \sin(\tau j) \right], \quad (5)$$

where $s = 2\pi y/P$ and $\tau = \Omega_{\text{bar}} t$, $\bar{Q} = Q_0$ is the averaged value of Q . The formula (5) is an adaptation for the simplified configuration under study of the generalized formula to transform the spatial harmonics stationary with respect to the rotor into unsteady time harmonics with respect to the stator (see [7]).

The results of unsteady effects on the T106 blades were obtained in the following order:

1. 2D SST RANS simulation of a cylinder (Bars2D mesh, see Tab. 1).
2. Extraction of profiles for SRS, their decomposition into N_h spatial harmonics.
3. 3D SST IDDES simulations with unsteady inflow BC (T106 mesh).

Also, several auxiliary scale-resolving computations were performed, as follows.

- A computation for the bars configuration (3D bars domain) was carried out to obtain the Reynolds stresses in the wake downstream the cylinder (the Bars3D mesh was used, see Tab. 1) that were used as a reference for evaluation of results.
- To evaluate the capability of reproducing turbulence in the cylinder wake with VSTG based on the parameters given by the RANS solution, computations on two meshes, Wake3Dc and Wake3Df, were performed in the domain, the input boundary of which was the same as for the T106 (at $x/C = -0.35$). A fragment of the computational domain is shown in Fig. 6 bottom (see bars-VSTG domain).

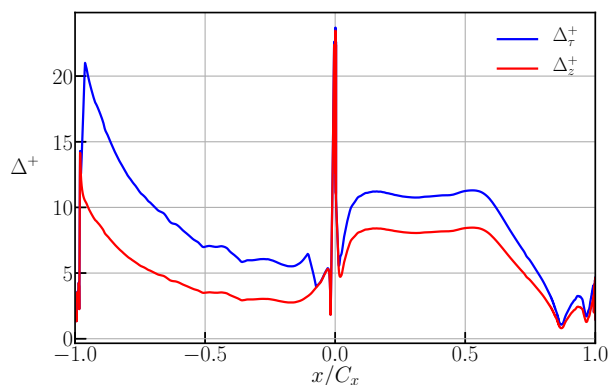
Parameters of the unstructured meshes used for computations are shown in Tab. 1. All 3D meshes were generated by extrusion of a 2D mesh (e.g., Bars3D is based on Bars2D) along the OZ axis with a constant step (denoted as Δ_z). 2D quad-dominant meshes are isotropic except for the near-wall region, where a proper number of layers with anisotropic elements were inserted to meet the $\Delta_{\text{wn},1}^+ < 1$ condition. Isotropic resolution with the corresponding maximum mesh step Δ_{max}^{xy} was maintained in the area specified as “ Δ_{max}^{xy} area” in Tab. 1. Also, the following designations are used in Tab. 1: N_n and $N_{n,2D}$ are the total numbers of nodes in the 3D and 2D meshes, respectively; N_z is the number of cells in the spanwise direction.

IDDES was used for all scale-resolving computations. The RANS regime of IDDES was forced from the input boundary down to the VSTG region. Otherwise, the RANS solution was damped fairly quickly by operating in LES mode. The VSTG zone $-0.31 \leq x/C \leq -0.275$ is fixed for all computations where it was used, the reference nodes are located $0.03C$ upstream the source area. Downstream the VSTG zone the IDDES operates in the LES regime, including the near-wall regions. Distributions of mesh steps (in wall-law variables) along the T106 blade surface from the unsteady simulation are presented in Fig. 7. It is evident from this that the mesh has sufficient resolution for WRLES. The upwind EBR3 scheme was used for RANS simulations,

Table 1. Parameters of meshes for T106 LPT related computations

Mesh	N_n	$N_{n,2D}$	N_z	Δ_z/C	Δ_{\max}^{xy}/C	Δ_{\max}^{xy} area
Bars2D	0.282M	–	–	–	$1.5 \cdot 10^{-3}$	$-1.05 \leq x/C \leq 0.35$
Bars3D	14.4M	0.282M	50	$1.5 \cdot 10^{-3}$	$1.5 \cdot 10^{-3}$	$-1.05 \leq x/C \leq 0.35$
Wake3Dc	3.68M	0.072M	50	$1.5 \cdot 10^{-3}$	$3 \cdot 10^{-3}$	$0.35 \leq x/C \leq 0.35$
Wake3Df	6.76M	0.133M	50	$1.5 \cdot 10^{-3}$	$1.5 \cdot 10^{-3}$	$0.35 \leq x/C \leq 0.35$
T106	18M	0.175M	100	$1.5 \cdot 10^{-3}$	$3 \cdot 10^{-3}$	$0.35 \leq x/C \leq 1.5$

while the lower-dissipation EBR4 scheme blended with EBR3 (with the coefficient 0.01) was exploited for SRS. The global CourantFriedrichsLewy (CFL) condition, $CFL_{\max} = 40$, was set for all scale-resolving computations. The local CFL values did not exceed 1 in the disturbed flow areas, which is needed to resolve well all relevant turbulent time scales. The time step $\Delta t_{\text{out}}/C$ slightly varied dynamically according to the global CFL condition, the average value was $1.23 \cdot 10^{-3}$. To accumulate the average flow statistics, we used averaging in time and in space along the homogeneous direction. The transient period of the simulations started from a preliminary 2D RANS solution is $8C/u_{\text{out}}$. After the transient period, the time integration interval of data accumulation is $30C/u_{\text{out}}$, which is more than sufficient to obtain converged flows parameters.


Figure 7. T106: distributions of wall-tangent Δ_{τ}^{+} and spanwise Δ_z^{+} mesh steps at the pressure ($x/C_x < 0$) and suction ($x/C_x \geq 0$) sides of the blade

All scale-resolving simulations were performed on NVIDIA V100 GPUs (900 GB/s). One timestep for simulation of the T106 blades cascade (unsteady regime) on 4 GPUs in the K60-GPU cluster (1 node with 2 Intel Xeon Gold 6142 CPUs and 4 GPUs) takes approximately 0.9 s of wall clock time. Consequently, it takes about 2 hours to simulate the period $10C/u_{\text{out}}$. Note that all VSTG nodes (their number is about 1.5% of the total number of nodes) belong to the first MPI domain (of four), so all source-related operations are performed by only one GPU (for four). The number of STG modes is 167.

4.2. Results

The results of the computations preceding SRS of the T106 blades cascade are presented in Figures 8 and 9: profiles of the Reynolds stresses are shown in Fig. 8, P_t and k distributions are presented in Fig. 9 (here $p_{\text{ref}} = \rho_{\text{ref}} u_{\text{ref}}^2$, where ρ_{ref} is the density at the outlet of the blades

cascade). The latter contains approximations based on spatial Fourier decomposition depending on the number of harmonics N_h too. The cross section $x/C = -0.35$ corresponds to the inlet boundary for the T106 domain (and for the bars-VSTG domain too), $x/C = -0.1$ is a section slightly upstream the leading edge of the blade. It is clearly seen that the Reynolds stresses obtained using RANS differ from the SRS results, which we consider as a reference. The shape of the graphs and peak values in Fig. 8 correlate well, whereas the main discrepancy lies in the region outside the center of the wake: turbulence levels are much higher there. Underestimation is related to limitations of the SST RANS model to predict flow characteristics past bluff bodies such as a round cylinder: presence of coherent structures and their downstream evolution is not considered correctly. However, shear layers characteristics downstream streamlined bodies (e.g., aerodynamic profiles or blades of rotating machines) are usually captured more accurately by Boussinesq-type turbulence models. Comparing the results obtained on the meshes Wake3Dc and Wake3Df, we conclude that the resolution of the Wake3Dc mesh is sufficient to provide adequate turbulence generated by the VSTG, the parameters of which are set based on the RANS solution. Note that the Wake3Dc mesh has the same resolution as the T106 one.

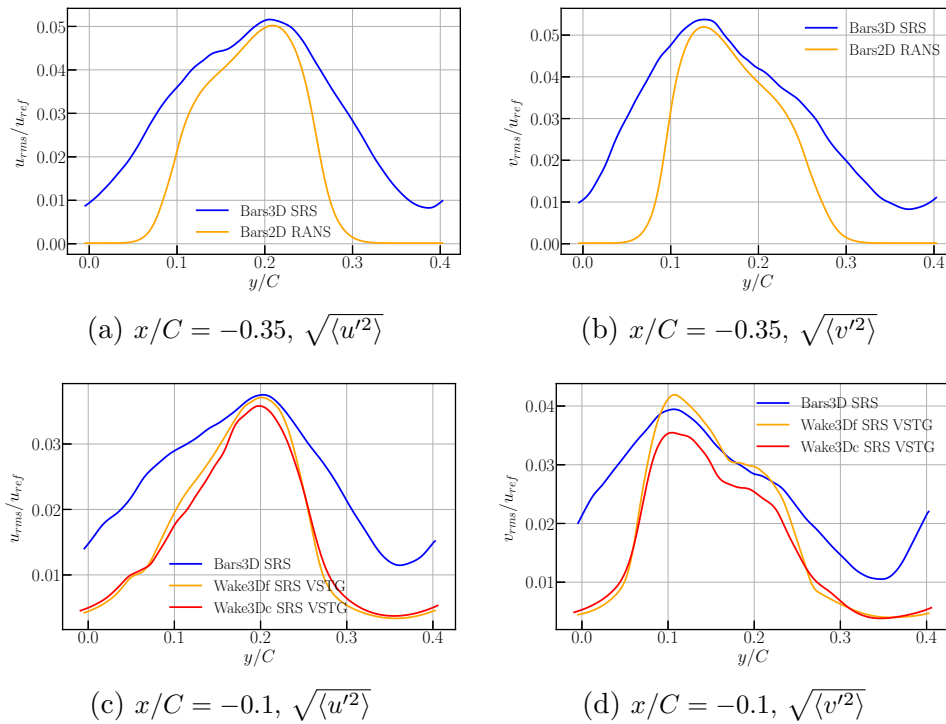


Figure 8. Bar results: profiles of normal Reynolds stresses (rms values)

Evaluating the graphs in Fig. 9, it can be seen that actual distributions of fields are approximated quite accurate by spatial harmonics starting from $N_h = 5$. After this value the difference between restored functions lies in the region outside peaks. We applied $N_h = 15$ to set unsteady BC for the T106 computation. Note that there are deviations of the approximated functions with values less than zero for turbulence kinetic energy, that is not appropriate. We limited the k values reconstructed through the sum of harmonics to zero from below to solve this problem.

Distributions of vorticity magnitude $|\Omega|$ at three consecutive time instants with a step $0.615C/u_{\text{out}}$ are shown in Fig. 10. It can be seen that artificial pulsations within the VSTG quickly transform into plausible resolved turbulence at a distance of about 2-3 thicknesses of

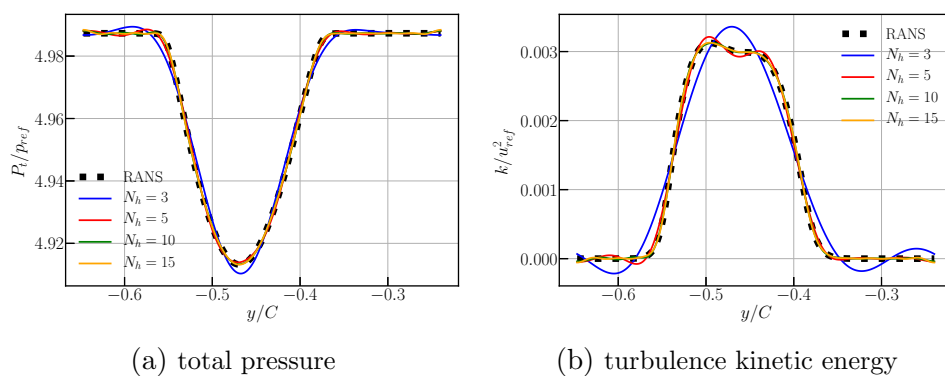


Figure 9. Bar results: profiles of variables – actual and reconstructed by the corresponding number of harmonics N_h

the source zone downstream. These wakes interfere with both pressure and suction sides of the blade. The boundary layer at the suction side states predominantly laminar except for a very small region located in close proximity to the trailing edge downstream the reattachment after a bubble-type LT transition (it is almost indistinguishable from the visualizations shown in Fig. 10). On the pressure side, near-wall turbulence appears after interference with the tails of periodic wakes.

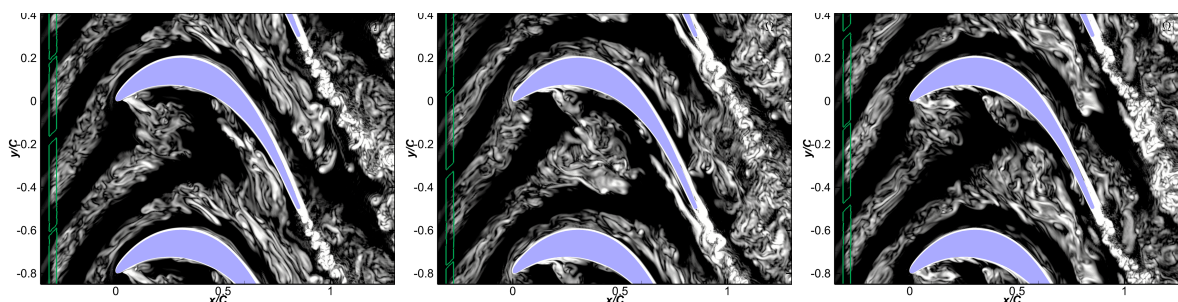


Figure 10. T106: distributions of vorticity magnitude at three consecutive time instants with a step $0.615C/u_{out}$

The effect of unsteady periodic perturbations is clearly manifested in the distributions of pressure C_p coefficient and friction C_f coefficient (for the suction side only) presented in Fig. 11. First of all, we note good agreement with the experimental data for both regimes, with zero turbulence level at the inlet (denoted as “SRS steady”) and with unsteady perturbations (“SRS VSTG unsteady”). The presence of the so-called bubble laminar turbulent (LT) transition on the suction side of the blade characterizes the first regime. There is also a small laminar bubble near the leading edge (see the C_f distribution of SRS steady in Fig. 11 c). As for the unsteady regime, the wakes interfere with the blade, causing the LT transition zone to move closer to the trailing edge and the recirculation zone to become noticeably smaller. In this case, the separation near the leading edge disappears completely. The LES simulation of the regime with unsteady perturbations from [11] predicted the absence of a bubble near the trailing edge, i.e., the transition becomes a bypass rather than of a bubble type. As a consequence, their results are in better agreement with the experiment in the region $x/C_x > 0.6$. But the flow over the bars was reproduced more “realistic” in [11]: pulsations were not simulated artificially. Therefore, we attribute the lower accuracy of our results to the limited accuracy of the RANS solution on

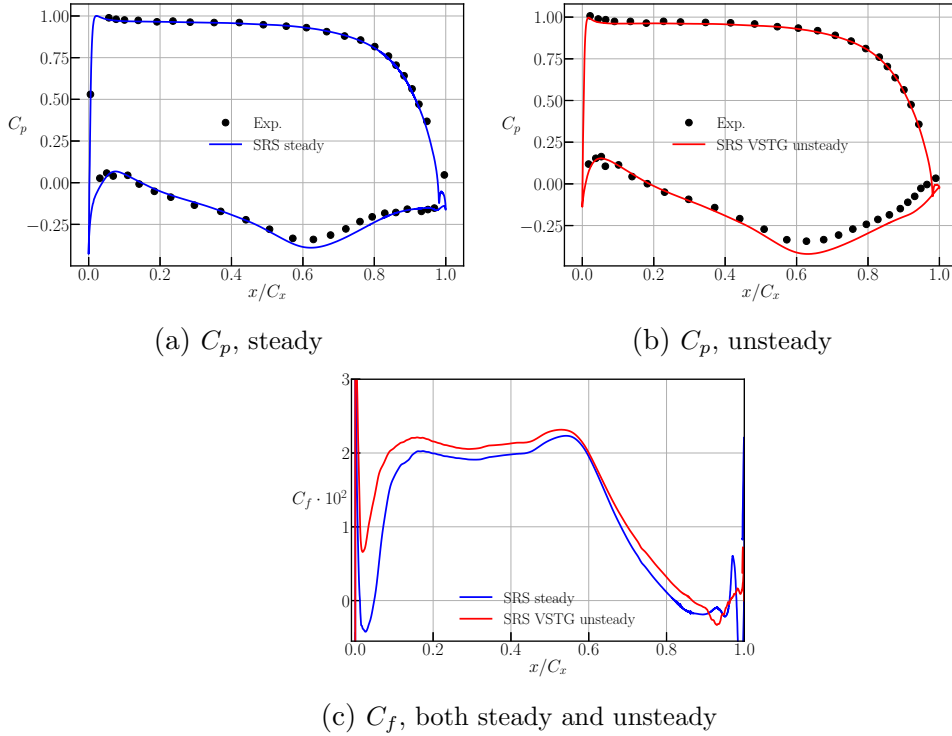


Figure 11. T106 results: averaged distributions of pressure (C_p) and friction (C_f) coefficients

the basis of which the pulsations are generated and, in general, to the difficulty in reproducing turbulence with the presence of specific coherent structures using the generator we apply. This is despite the computational meshes used, which are close in resolution (our mesh to the mesh from [11]). However, in turbomachines, the blade wakes are closer to the mixing layers, for the artificial reproduction of which the STG is better adapted.

Conclusion

The methodology for studying the effects associated with periodic unsteady impact from the preceding row in turbomachines using scale-resolving simulation is presented. It considers the two-stage procedure of an investigation: RANS simulation of an entire turbomachine at the first stage; SRS of the row under consideration at the second. The methodology is based on the following methods and technologies, which are implemented in the NOISEtte computational algorithm.

- Nonlinear harmonics method which is used to obtain unsteady inflow parameters for SRS in a preliminary RANS computation.
- Hybrid RANS-LES IDDES approach for scale-resolving simulation of the row under detailed study.
- Dynamic VSTG to reproduce unsteady periodic turbulent perturbations within the SRS stage.

The VSTG is adapted to the capabilities of dynamically varying turbulent flow downstream of the source region. All computationally intensive calculations are conducted using the GPU version of the NOISEtte code following its heterogeneous MPI+OpenMP+OpenCL parallelization model. All possible operations of scale-resolving computations are efficiently performed on

graphic accelerators. The primary issue is attributed to the fact that, due to the locality of the source region and the substantial computational load associated with its operation, a load imbalance arises in the context of MPI parallelism (only one GPU of multiple GPUs could be loaded with VSTG-related operations).

The advantage of the methodology is that the most computationally intensive part, namely, scale-resolving simulation, is carried out only for one domain representing a periodic sector of a row, the characteristics which are studied in detail. At the same time, the use of NLH allows to obtain plausible inflow conditions representing the unsteadiness of adjacent rows for realistic turbomachines.

The simulation of unsteady effects at the T106 LPT cascade was performed to demonstrate applicability of the methodology presented. The obtained results correlate well with the experimental data for both simulated regimes, with zero turbulence level at the inlet and with unsteady perturbations. However, it was not possible to exactly reproduce the effect of the periodic wakes on the T10C blades cascade, likely due to the insufficiently accurate reproduction of the flow downstream the cylinders using VSTG. It is therefore evident that the capabilities of the proposed technique are constrained by the capabilities of the synthetic turbulence generator that is utilised. In the context of realistic turbomachines, the blade wakes are in closer proximity to the mixing layers. And the VSTG is better adjusted to the artificial reproduction of them. Consequently, the proposed technology appears to be a potentially viable solution.

Subsequent research will address the potential for reducing the computational cost of operations associated with VSTG. Also, there is a strong interest in the full application of the developed technology, i.e., on a realistic turbomachinery problem (multi-stage turbomachine), where the non-simplified NLH technology is employed at the RANS stage.

Acknowledgements

The research is carried out using the equipment of the shared research facilities of HPC computing resources at Lomonosov Moscow State University [30], the equipment of Shared Resource Center of KIAM RAS (<http://ckp.kiam.ru>). The authors thankfully acknowledge these institutions.

This paper is distributed under the terms of the Creative Commons Attribution-Non Commercial 3.0 License which permits non-commercial use, reproduction and distribution of the work without further permission provided the original work is properly cited.

References

1. NASA Turbulence Modeling Resource. 2DML: 2D Mixing Layer Validation Case. https://turbmodels.larc.nasa.gov/delvilleshear_val.html
2. Abalakin, I.V., Bakhvalov, P.A., Bobkov, V.G., *et al.*: NOISEtte CFD&CAA Supercomputer Code for Research and Applications. *Supercomputing Frontiers and Innovations* 11(2), 78–101 (Aug 2024). <https://doi.org/10.14529/jsfi240206>
3. Abalakin I., Bakhvalov P., Kozubskaya, T.: Edge-based reconstruction schemes for unstructured tetrahedral meshes. *International Journal for Numerical Methods in Fluids* 81, 331–356 (2016). <https://doi.org/10.1002/flid.4187>

4. Bakhvalov, P.A., Surnachev, M.D.: Method of averaged element splittings for diffusion terms discretization in vertex-centered framework. *Journal of Computational Physics* 450, 110819 (Feb 2022). <https://doi.org/10.1016/j.jcp.2021.110819>
5. Burgos, M.A., Contreras, J., Corral, R.: Efficient edge-based rotor/stator interaction method. *AIAA Journal* 49(1), 19–31 (Jan 2011). <https://doi.org/10.2514/1.44512>
6. Delville, J., Bellin, S., Garem, J.H., Bonnet, J.P.: Analysis of Structures in a Turbulent, Plane Mixing Layer by Use of a Pseudo Flow Visualization Method Based on Hot-Wire Anemometry, pp. 251–256. Springer Berlin Heidelberg (1989). https://doi.org/10.1007/978-3-642-83822-4_38
7. Duben, A.P., Zagitov, R.A., Shuvaev, N.V.: Nonlinear harmonics method for supercomputer simulations of fluid dynamics in turbomachines with higher accuracy on unstructured meshes. *Lobachevskii Journal of Mathematics* 45(7), 3007–3016 (Jul 2024). <https://doi.org/10.1134/s1995080224603916>
8. Duben, A., Gorobets, A.: Scale-resolving simulation of a low-pressure turbine on hybrid supercomputers. *Computers & Fluids* 265, 105984 (Oct 2023). <https://doi.org/10.1016/j.compfluid.2023.105984>
9. Duben, A., Gorobets, A., Soukov, S., *et al.*: Supercomputer Simulations of Turbomachinery Problems with Higher Accuracy on Unstructured Meshes, pp. 356–367. Springer International Publishing (2022). https://doi.org/10.1007/978-3-031-22941-1_26
10. Duben, A., Zagitov, R., Shuvaev, N., Marakueva, O.: Towards an Adaptation of the Nonlinear Harmonics Method Realized in an Unstructured Flow Solver for Simulation of Turbomachinery Problems on Supercomputers, pp. 253–266. Springer Nature Switzerland (2025). https://doi.org/10.1007/978-3-031-78459-0_19
11. Fiore, M., Gojon, R., Sáez-Mischlich, G., Gressier, J.: LES of the T106 low-pressure turbine: Spectral proper orthogonal decomposition of the flow based on a fluctuating energy norm. *Computers & Fluids* 252, 105761 (Feb 2023). <https://doi.org/10.1016/j.compfluid.2022.105761>
12. Gorobets, A.: Adapting a Scientific CFD Code to Industrial Applications on Hybrid Supercomputers. *Supercomputing Frontiers and Innovations* 9(4), 49–54 (Nov 2022). <https://doi.org/10.14529/jsfi220405>
13. Gorobets, A., Bakhvalov, P.: Heterogeneous CPU+GPU parallelization for high-accuracy scale-resolving simulations of compressible turbulent flows on hybrid supercomputers. *Computer Physics Communications* 271, 108231 (Dec 2022). <https://doi.org/10.1016/j.cpc.2021.108231>
14. Guseva, E.K., Garbaruk, A.V., Strelets, M.K.: Assessment of Delayed DES and Improved Delayed DES Combined with a Shear-Layer-Adapted Subgrid Length-Scale in Separated Flows. *Flow, Turbulence and Combustion* 98, 481–502 (2017). <https://doi.org/10.1007/s10494-016-9769-7>

15. Hu, S., Zhou, C., Xia, Z., Chen, S.: Large Eddy Simulation and CDNS Investigation of T106C Low-Pressure Turbine. *Journal of Fluids Engineering* 140(1) (Oct 2017). <https://doi.org/10.1115/1.4037489>
16. Magomedov, A.R., Gorobets, A.V.: Heterogeneous Implementation of Preconditioners Based on Gauss-Seidel Method for Sparse Block Matrices. *Computational Mathematics and Modeling* 33(4), 438–442 (Oct 2022). <https://doi.org/10.1007/s10598-023-09585-2>
17. Menter, F.R.: Two-equation eddy-viscosity turbulence models for engineering applications. *AIAA Journal* 32(8), 1598–1605 (Aug 1994). <https://doi.org/10.2514/3.12149>
18. Michelassi, V., Wissink, J., Rodi, W.: Analysis of DNS and LES of Flow in a Low Pressure Turbine Cascade with Incoming Wakes and Comparison with Experiments. *Flow, Turbulence and Combustion* 69, 295–329 (2002). <https://doi.org/10.1023/a:1027334303200>
19. Mockett, C., Fuchs, M., Garbaruk, A., *et al.*: Two non-zonal approaches to accelerate RANS to LES transition of free shear layers in DES. In: *Progress in Hybrid RANS-LES Modelling*, pp. 187–201. Springer International Publishing (2015). https://doi.org/10.1007/978-3-319-15141-0_15
20. Saad, Y.: *Iterative methods for sparse linear systems*. Society for Industrial and Applied Mathematics, Philadelphia (2003)
21. Sandberg, R.D., Michelassi, V.: The current state of high-fidelity simulations for main gas path turbomachinery components and their industrial impact. *Flow, Turbulence and Combustion* 102(4), 797–848 (Feb 2019). <https://doi.org/10.1007/s10494-019-00013-3>
22. Sandberg, R.D., Michelassi, V., Pichler, R., *et al.*: Compressible Direct Numerical Simulation of Low-Pressure Turbines—Part I: Methodology. *Journal of Turbomachinery* 137(5) (May 2015). <https://doi.org/10.1115/1.4028731>
23. Shorstov, V.A.: Possibilities and Restrictions on the Use of the Zonal RANS-IDDES Approach to Calculate Fan Noise. *Mathematical Models and Computer Simulations* 15(2), 265–276 (Apr 2023). <https://doi.org/10.1134/s2070048223020163>
24. Shur, M., Strelets, M., Travin, A., *et al.*: Improved Embedded Approaches. *Notes on Numerical Fluid Mechanics and Multidisciplinary Design* 134, 65–69 (2017). https://doi.org/10.1007/978-3-319-52995-0_3
25. Shur, M.L., Spalart, P.R., Strelets, M.K., Travin, A.K.: Synthetic Turbulence Generators for RANS-LES Interfaces in Zonal Simulations of Aerodynamic and Aeroacoustic Problems. *Flow, Turbulence and Combustion* 93, 63–92 (2014). <https://doi.org/10.1007/s10494-014-9534-8>
26. Shur, M.L., Spalart, P.R., Strelets, M.K., Travin, A.K.: An enhanced version of DES with rapid transition from RANS to LES in separated flows. *Flow, Turbulence and Combustion* 95(4), 709–737 (2015). <https://doi.org/10.1007/s10494-015-9618-0>
27. Stadtmüller, P.: Investigation of wake-induced transition on the LP turbine cascade T106A-EIZ. Tech. Rep. Fo 136/11, Version 1.1, DFG-Verbundprojekt (2002)

28. Suzuki, T., Spalart, P.R., Shur, M.L., *et al.*: Unsteady simulations of a fan/outlet-guide-vane system: Broadband-noise computation. *AIAA Journal* 57(12), 5168–5181 (Dec 2019). <https://doi.org/10.2514/1.j058177>
29. Tyacke, J., Vadlamani, N.R., Trojak, W., *et al.*: Turbomachinery simulation challenges and the future. *Progress in Aerospace Sciences* 110, 100554 (Oct 2019). <https://doi.org/10.1016/j.paerosci.2019.100554>
30. Voevodin, V., Antonov, A., Nikitenko, D., *et al.*: Supercomputer Lomonosov-2: Large scale, deep monitoring and fine analytics for the user community. *Supercomput. Front. Innov.* 6(2), 4–11 (2019). <https://doi.org/10.14529/jsfi190201>
31. Voroshnin, D.V., Marakueva, O.V., Muraveiko, A.S.: Modeling unsteady phenomena in an axial compressor. *Mathematical Models and Computer Simulations* 12(3), 413–421 (May 2020). <https://doi.org/10.1134/s2070048220030187>
32. Wu, X., Durbin, P.A.: Evidence of longitudinal vortices evolved from distorted wakes in a turbine passage. *Journal of Fluid Mechanics* 446, 199–228 (Oct 2001). <https://doi.org/10.1017/s0022112001005717>